

Methods of Fabrication and Testing for Resonating Micro-Rings and Disks as Sensors

Camille Baird

A senior thesis submitted to the faculty of
Brigham Young University
in partial fulfillment of the requirements for the degree of
Bachelor of Science

Robert Davis, Advisor

Department of Physics and Astronomy
Brigham Young University
April 2019

ABSTRACT

Methods of Fabrication and Testing for Resonating Micro-Rings and Disks as Sensors

Camille Baird

Department of Physics and Astronomy, BYU

Bachelor of Science

Porous micro-resonators show promising results for applications in chemical and bio-sensing. Rings and disks resonating in the wine-glass mode or radial contour mode have been designed and fabricated using a highly tunable microfabrication process to undergo further testing for quality factors and viability for sensing applications in fluid environments. Narrow anchors from the resonating structure to mounted pads have been placed at nodal points of the modes of vibration to reduce clamping losses during testing.

Table of Contents

List of Figures

Chapter 1

Introduction

1.1 Introduction	6
------------------------	---

Chapter 2

Review of Microelectromechanical Resonators

2.1 Quality Factor	7
2.2 Damping Losses.....	8
2.3 Modes of Vibration and Geometric Configurations.....	8
2.4 Transduction Methods.....	9

Chapter 3

Rings and Disks as Chemical Sensors

3.1 Mass Sensing	10
3.4 Advantages of Porous Sensors.....	11
3.5 Previous Work on Porous Cantilever Sensors.....	12
3.6 Current Work	12

Chapter 4

Experimental Methods

4.1 Introduction to the CNT-M process	13
4.1.1 Mask and Resonator Device Design.....	20
4.1.2 Wafer Processing and Preparation for Growth	13
4.1.3 Growth and Infiltration	14
4.1.4 Device Release and Mounting	15
4.2 Material Characterization	19

4.3 Device Characterization	20
4.3.1 Model for Circular Disks	21
4.3.2 Model for Annular Rings	22
4.4 Electro-Thermal Actuation.....	23
4.5 Resonance Testing	23

Chapter 5

5.1 Device Results	25
5.2 Method of Release Results	27
5.3 Resonance Predictions.....	22
5.4 Discussion.....	29

Bibliography

List of Figures

Figure 1: An illustrative example of a CNT structure for Method 1 release process	16
Figure 2: An illustrative example of a CNT structure prepared for various release processes.....	17
Figure 3: An illustrative example of the process outlined by Method 5 for release	18
Figure 4: Snapshots of the resonator mask design file showing a variety of ring and disk structures.....	21
Figure 5: An image taken by a scanning electron microscope of a ring resonator.	25
Figure 6: A photograph of an array of CNT-M disk resonators.....	26
Figure 7: a photograph of a CNT-M disk resonator mounted to a silicon substrate via carbon tape.....	27
Figure 8: A before and after photograph of a ring resonator with partial scratching.....	28
Figure 9: An SEM image of the inside and outside of a ring of a CNT-M structure.....	28
Figure 10: an SEM image of the anchor and pad features of a CNT-M ring resonator.....	29

Chapter 1

1.1 Introduction

Microelectromechanical systems (MEMS) offer significant advantages as resonators due to their small size, large frequency-quality factor product, low power consumption, and agile integration into other systems and processes.[1] Microelectromechanical resonators have shown promising results in a variety of applications, including mass sensing, timing devices, and radio frequency processing. [2] Rings and disks have shown a particular aptitude for their ability to maintain high quality factors during mass sensing, even in fluidic environments.[1] [3] [4] It has been shown that the best mass sensors are structures that have a high-aspect ratio, low mass, but still have a large surface area. However, physical limits of previously used materials have capped the optimization of these sensors. Because of the unique electrical and mechanical properties exhibited by resonators fabricated using a carbon nanotube templated microfabrication (CNT-M) process, they are an ideal material for creating highly accurate and sensitive resonators as applied to mass sensing.[5] Microelectromechanical disks and rings comprised of CNT-M material were designed, fabricated and theoretically and experimentally characterized to investigate the quality factor as an indicator for the success of the devices in mass sensing.

Chapter 2

Review of Properties of Microelectromechanical Resonators

2.1 Quality Factor

The quality factor is a property of the oscillator; it is considered as the natural frequency of vibration. Resonators with high quality factors take a long time to stop resonating or oscillating, while low quality factors are characteristic of resonators that “ring down” very quickly. Therefore, a large quality factor indicates the resonator will only resonate within a narrow range of frequencies, meaning they exhibit a sharp peak of oscillation, referred to as the resonance peak, when swept through a range of frequencies. Low quality factors indicate that the structure will resonate with a broad range of frequencies. The best sensors have high quality factors and thus a sharp resonance peak. From experimental data or a modeled fit, the quality factor can be estimated by measuring the resonance peak’s full width at half maximum and dividing by the resonant frequency. [1]

$$Q = \frac{f_0}{\Delta f} \quad (2.1)$$

The quality factor may be defined as the ratio of the energy stored over the energy dissipated per cycle.

$$Q = 2\pi \left(\frac{\text{Energy stored}}{\text{Energy dissipated per cycle}} \right) \quad (2.2)$$

Thus, the quality factor may be increased as the energy dissipated per cycle, also known as damping loss, is minimized.

2.2 Damping Losses

There are many causes for energy to be lost in the system. Some of the most common damping losses are due to environment viscosity, anchors geometry, and material losses. [6] Viscous losses occur as resonating systems have large surface to volume ratios, variable or high gas pressures or other fluidic environments. Most resonator structures are required to be anchored to a substrate for measurement and to drive the oscillatory motion. These can be mitigated when the cross-sectional dimensions of the anchors to the resonator are reduced, when the center of the anchors are aligned to the nodal points of the mode of vibration, and when the anchor length is proportional to the acoustic wavelength produced by the frequency at which the device is driven. Material losses can be observed in the form of heat energy losses or thermo-elastic damping.

2.3 Modes of Vibration and Geometric Configurations

The quality factor has been shown to be affected by energy or damping losses caused by the mode of vibration, the geometric shape, anchor geometry, and the environment in which the resonator is operated. Common modes of vibration include flexural, torsional, shear and bulk mode vibrations. [7] Flexural modes can be similar to transverse standing waves, wherein the structural displacement is orthogonal to the bending stress. In the torsional mode of vibration, a rotational displacement occurs, wherein a shear-stress is observed as the dominant stress. Bulk modes can be characterized as standing longitudinal waves with sub-modes observed based on various geometries of the resonator. The resonant frequencies of bulk mode resonators can be described generally by the following equation:

$$f_{bulk} = \frac{\beta}{\lambda} \sqrt{E_{bulk}/\rho} \quad (2.3)$$

It is interesting to note that thermo-elastic damping is not significant in the shear or bulk modes of vibration. Bulk modes also resonate at higher frequencies for similar dimensions when compared to flexural modes. Common geometries or shapes include beams, square plates, combs, circular disks, annular rings and even coupled devices comprised of multiple resonators formed in one or more geometric shapes. The highest quality factors are achieved as a resonator is designed with an optimal combination of resonant frequency, device and anchor geometry, and mode of vibration to minimize damping losses.

2.4 Actuation Methods

To make a meaningful measurement of the quality factor of a resonator, the device should be driven at its resonance frequency in the desired mode of vibration. One common actuation method is brought about by capacitively driving the resonator, wherein a voltage is applied between two conducting plates separated by an insulator. Another method of transduction is achieved via piezo-electric materials which allow for the direct conversion of electric polarization into mechanical stress. [8] In the case of capacitive and piezo-electric methods, the device can be driven and the vibrational frequency can be measured within the same electrical system. A third method to drive the resonator is thermal actuation, which is performed by passing an alternating current through a set of heat resistors in contact with the resonator. A thermal wave is created within the resonating structure and is manipulated so that the frequency of the thermal wave is equivalent to the mechanical resonant frequency of the device. [9]

Chapter 3

Rings and Disks as Chemical Sensors

3.1 Mass Sensing

One application of resonators is in resonant mass or gravimetric sensing based on changes in the effective mass of the resonator. A detected shift in the resonant frequency can be correlated to the amount of an analyte interacting with the resonator. Thus, resonant mass sensors can be employed in determining particle concentration, deposition rate, chemical sensing, and bio-sensing. Looking at Equation (3), to achieve high mass sensitivity, the resonator should be designed to oscillate at a high resonant frequency while maintaining a low effective mass. [2] Additionally, the resonator should have a high surface area to increase the threshold of saturation of analyte onto its surface. To provide selectively of analyte interaction, the resonator is coated with a thin chemical film or protein that selectively binds to the target chemical or biomolecule.

3.2 State of Current Devices

Resonant structures that oscillate in bulk modes of vibrations have been shown to reach higher resonant frequencies with higher quality factors. In the case of a square micro-resonator, the bulk mode was recorded to have a quality factor approximately 10x larger than the quality factor measured in the extensional mode.[10] In the case of a circular disk comprised of single crystal silicon was excited in a bulk mode referred to as the wine glass mode and was found to have a quality factor of 1,900,000 at 5.43 MHz.[3] A poly-silicon disk driven in the wine-glass mode was found to be 145,780 at 60 MHz.[11] Another wine glass disk comprises of single crystal silicon was found to have a quality factor of 45,742 at 149.3 MHz.[12] An annular ring

vibrating in the radial contour mode achieved a quality factor of 14,603 at 1.2 GHz, one of the highest resonant frequencies recorded with a promising quality factor.[4]

Although high frequency-quality factor products have been achieved, these promising metrics decrease significantly in gaseous or liquid environments. In one example, a rotational mode whole disk was observed to have a resonant frequency of 5724 KHz in air with a quality factor of 1140. When the disk was operated in liquid, the resonant frequency was observed to be 5703 KHz with drop in quality factor to 284. Previously, the highest quality factors in liquid environments were found to be within the range of 2-94, with in-plane modes achieving the higher end of the quality factor range.[13] Recent research work is being done to explore the possibility of increasing that quality factor range in liquid environments utilizing porous structures as the framework for micro-resonators.

3.4 Advantages of Porous Sensors

Porous resonators have shown promising preliminary results in having many advantages over solid structured resonators.[5] Porous structures have a significant increase in surface areas as compared to solid devices of similar dimensions. Since one of the limiting metrics of sensitivity of a resonator in chemical or bio-sensing is the amount of area available for molecule adsorption, porous resonators offer a major advantage to increasing the surface area while maintaining a lower overall volume. Uniform porosity also allows for a network of fluidic diffusion paths throughout the entirety of the structure. Methods to increase porosity have included increasing the roughness of the surface of a solid device and integrating a thin porous layer onto the outer surface of the resonator, achieving up to a 261% improvement in resonator sensitivity.[14] Furthermore, the ratio of the overall mass of the resonator to the mass of the

desired analyte should remain low to achieve sensitive measurements. However, while low-aspect ratio devices maintain a low mass ratio, it is accompanied by a low energy output in their resonant mode which decreases the quality factor in fluid environments.

3.5 Previous Work on Porous Cantilever Sensors

Mechanically robust CI-CNT cantilevers were fabricated using a novel carbon nanotube templated microfabrication (CNT-M) process developed at Brigham Young University. [15] The structures formed were measured to show a high surface to area volume ratio, with tunable porosity and density parameters. Quality factors were observed to be between 100 and 1000 at atmospheric pressure in air at varying humidity levels.[5] It was reported that internal losses were not a dominant source of energy loss, with about half the damping coming from fluid damping and another portion coming from clamping losses.

3.6 Current Work

The work presented in this thesis serves to expand on the foundational results of the work done by Noyce. et al, to explore the further reduction of non-fluid losses (clamping losses and thermoelastic damping)[5] by designing resonators in high-aspect ratio disk and ring geometries having narrow anchors located at vibrational nodal points.[16] The disk and ring resonators presented in this work have been designed with anchors at nodes occurring in the wine-glass mode of vibration in hopes of decreasing clamping losses. The wine-glass mode is characterized by in-plane oscillations which should offer lower fluid damping as compared to the out of plane motion observed by the aforementioned porous cantilevers.

Chapter 4

Experimental Methods

4.1 Introduction to the CNT-M process

The CNT-M fabrication method offers a tunable and scalable microfabrication method of manufacturing porous micro-resonators. The CNT-M process relies on modifications to silicon semiconductor and MEMs fabrication using lithography and various layers of substrate deposition to achieve effective results. A patterned template of carbon nanotubes is grown on a silicon-based substrate wherein the density, and subsequent porosity, of the structure may be tuned by varying the time of post-growth infiltration of amorphous carbon. This method has also been shown to achieve very high aspect ratios, with growths up to 1mm in height.[17]

4.1.2 Wafer Processing and Preparation for Growth

A silicon wafer is initially prepared by underdoing a 250 W oxygen plasma etch for 2 minutes to clean the outer surface of the wafer. The wafer is placed directly into an E-beam evaporator to undergo an alumina deposition of about 50 nm. A deposition rate of approximately 2.5 Å/s can be achieved with a source of 40 mA. The wafer is then transferred to the oxygen plasma chamber for 5 minutes at 250W to increase growth rates.[18]

A positive photoresist layer comprising of 50 drops of AZ3330 and 4 drops of HDMS is spun at 5500 rpm for 60 seconds onto the deposited alumina layer. A soft bake of the wafer is performed on a heat plate at 90 °C for 60 seconds. The wafer is processed in a lithography aligner with a hard contact 10 second exposure with a 50 μm gap with the designed resonator mask. The wafer is then rinsed in fresh container of AZ300 MIF for 60 seconds, and then

immediately rinsed with de-ionized water on both sides of the wafer and dried with an inert gas. A deposition of a 4 nm layer of iron can be performed using a thermal-evaporator vacuum chamber. A deposition rate of approximately $.3 \text{ \AA/s}$ is observed at a temperature low of 19 K.

The wafer needs to be split into smaller substrate pieces to aid in the growth process. The photoresist, and accompanying iron layer, formed outside of the desired patterned CNT template is removed in a n-methyl pyrrolidone (NMP) bath in a heated sonicator for about 20 minutes. The wafer is then rinsed with water for 30 seconds and placed in a water bath.

4.1.3 Growth and Infiltration

A piece of the wafer having a patterned iron layer representing the ring or disk template of the resonator should be dried with an inert gas and placed into a quartz tube in a furnace. Argon is flushed through the system for 30 seconds. Hydrogen gas then flows through the closed chamber at 311 sccm flow for 3 minutes. The furnace is programmed to reach a temperature of $750 \text{ }^\circ\text{C}$ which causes the iron oxide to reduce to iron metal. The average time the furnace takes to heat up to $750 \text{ }^\circ\text{C}$ is approximately 12 minutes. Under high heat, thermal mobility of the surface layer allows the iron film to dissociate into nanoparticles on the alumina surface of the wafer.

When the furnace reaches the desired temperature, ethylene gas is allowed to flow at a rate of 338 sccm with the continuous hydrogen flow, supplying a carbon source to the system. The iron nanoparticles catalyze the decomposition of ethylene molecules and allow the thermally excited carbon atoms to form covalent bonds in chains of rings. The continuously growing lattice of covalently bonded carbon atoms forms the structure of a carbon nanotube. The longer the ethylene gas is allowed to flow, the taller the carbon nanotubes can grow. Once the desired growth height of the carbon nanotube forest, the ethylene gas is shut off, cutting off the carbon source.

The structure of newly grown carbon nanotubes is a highly porous system. For added structural stability or other binding purpose, the forest can be infiltrated or filled in with other materials such as amorphous carbon, nickel, copper, tungsten, silicon[19], silicon dioxide, or silicon nitride. The infiltration of amorphous carbon can be realized by the following process: The furnace is heated to 900 °C while hydrogen gas flows through the quartz chamber. At the now higher temperature, the hydrocarbon gas does not require a catalysis to facilitate the dissociation of the molecules into atoms. Thus, the carbon atoms deposit onto all previously formed structures. The level of infiltration is determined by the time the ethylene gas is allowed to flow at 900 °C.

4.1.4 Device Release and Mounting

To allow the circular resonator to oscillate in the desired mode of vibration, the entirety of the disk or ring and connected anchors must be released from the substrate while the pads remain in contact with or are bound to the substrate. There are several proposed methods that can be tested to achieve this configuration of the resonator. A few considerations to mention are that a carbon floor layer is left on the surface of the wafer from the amorphous carbon infiltration. Certain chemicals can be used to etch one or more of the wafer layers including the silicon, alumina, iron, carbon floor layer or other layer deposited during the fabrication process.

One method (Method 1: See Figure 1) of releasing the desired portion of the structure involves manually scribing/scratching around the disk or ring and anchor supports with a titanium tip which removes a small width of the carbon floor layer and exposes the iron and silicon layers underneath. The sample (substrate layers and carbon nanotube forest) can then be placed into a 30% by weight KOH bath heated to a range of 50-60 °C, wherein the KOH can etch underneath the desired portions of the resonator structure via the exposed portions of silicon.

Etch rates for 30% by weight KOH have been found to be between 15-25 microns/hour at 50-60 °C.[20] After soaking in KOH for the desired amount of time, the sample can then be transferred to a second water bath, and then soaked in an acetone bath. Acetone has a lower surface tension than water so when the resonators dry in air, they do not experience undo internal stress.

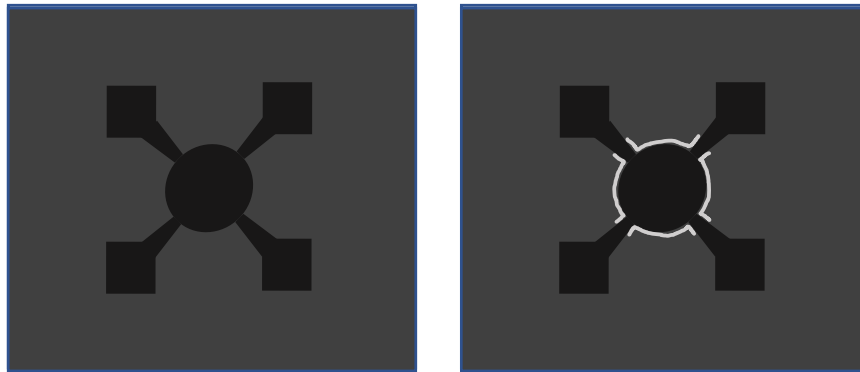


Figure 1: From left to right: An illustrative example of a CNT structure as fabricated on a silicon wafer using the CNT-M process; an illustrative example of manually scratching around the portions of the resonant structure to be released via a chemical etching bath.

A second sample (Sample 2) housing a larger ring underwent a similar release process (Method 2: See Figure 2), with the additional step of painting with cyanoacrylate around the outermost edges of the square pads as added protection against etching by the KOH bath. Another method comprises the steps (Method 3: See Figure 7) to re-mount and bond the pads of this sample and another set of fully released devices to a substrate base so as to allow the circular resonator to oscillate freely. The bonding could be carried out using a slow-cure epoxy on a heated plate. A full release can be facilitated by placing the sample of resonator disks in an oxygen plasma etch to remove the carbon floor layer and then released in a KOH bath.

The pads and all exposed wafer edges can be painted with cyanoacrylate (Method 4: See Figure 2). The wafer edges should be painted so that the entire device would not be released, but that the pads could remain bonded.

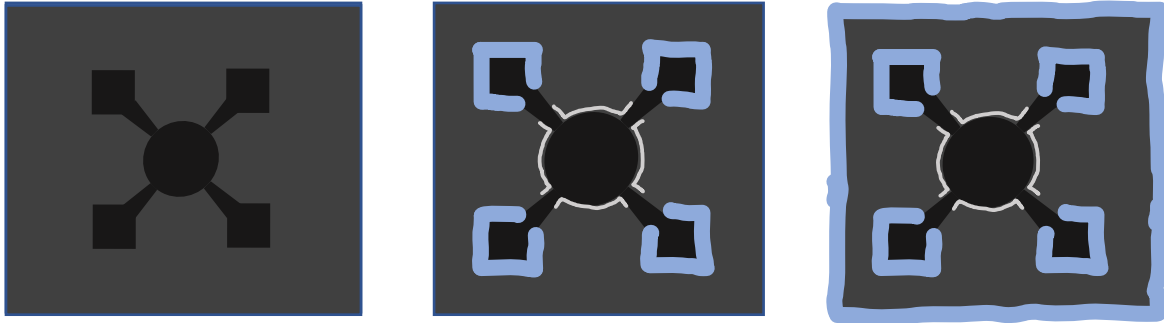


Figure 2: From left to right: an illustrative example of a CNT structure as fabricated onto a silicon wafer via the CNT-M process; an illustrative example of Method 2 comprising: manually etching around the desired portions of the structure for release and painting cyanoacrylate around the edges of the anchor pads to protect from etching and release during a chemical bath; an illustrative example of Method 4 comprising the steps of Method 2 with the addition of painting around the outer edges of the sample substrate to further prevent etching during the chemical bath.

Other methods that should be explored to release the devices from the silicon wafer include a back-side etch (Method 5: See Figure 3) in which a portion of the underside of the silicon wafer is painted with epoxy or other material that cannot be etched by KOH and then a KOH bath is allowed to etch through a middle portion of the silicon wafer directly underneath the disk portion of the resonator, releasing the device from underneath.

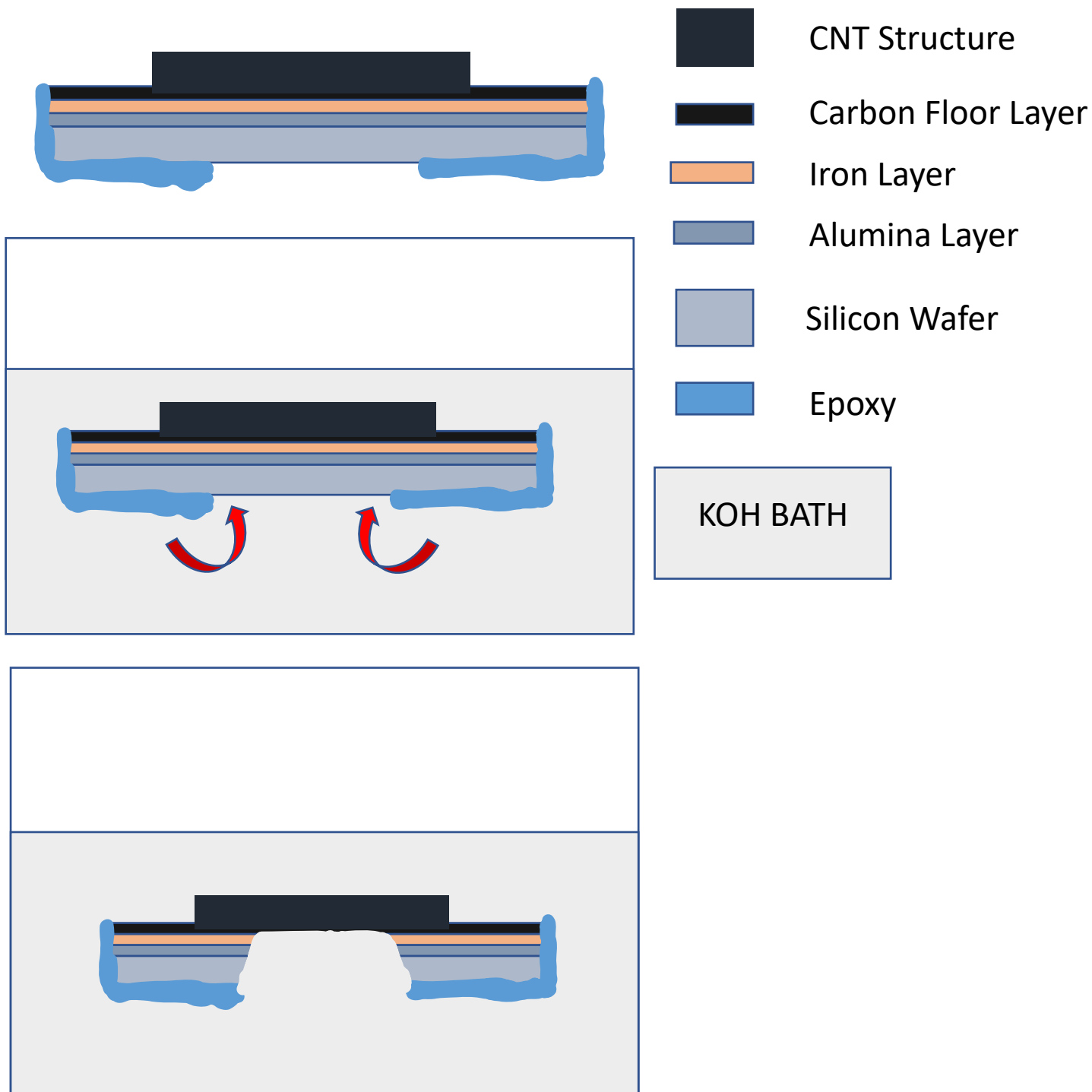


Figure 3: From top to bottom, an illustration of the steps of Method 5 comprising painting with an epoxy around the bottom of a silicon wafer leaving the center exposed; placing the sample into a KOH bath; wherein the KOH etches the silicon from the back-side to release the center of the resonator.

Another method (Method 6) includes designing the mask so that the devices can be formed with larger pads so that after the carbon floor layer is removed and the sample is placed in the KOH bath, the desired portions of the circular resonator and anchors will be etched. Parts of the pads will also be etched, but because of their proportionately larger size to the circular resonator dimensions, parts of the pads will remain bonded to the silicon wafer.

A promising method (Method 7) of release includes an additional step in the lithography process. A patterned layer of tungsten would be deposited underneath the iron layer where the circular disk and anchors are to be grown. After subsequent fabrication techniques as discussed above were followed, the sample would be placed into an oxygen plasma etch to remove the carbon floor layer and iron layer surrounding the resonator device. The sample could then be placed into a hydrogen peroxide bath which is designed to etch only the tungsten layer. Because hydrogen peroxide does not etch alumina or silicon, the device can be left in the chemical etch bath without the undue worry of sensitive time factors involved with the KOH etching which can release the device in its entirety.

4.2 Material Characterization

The height of each device was measured via a micrometer and via a microscope. The in-plane dimensions of the resonator, anchors and pads are determined by the initial design of the resonator mask used in the photolithography steps of fabrication. The devices that were fully released from the silicon substrate were measured by a microbalance to determine the mass of each device before re-mounting the device pads onto a base substrate.

Infiltration of amorphous carbon has been shown to increase the material density, with approximately 100 kg/m^3 with no infiltration, increasing to 400 kg/m^3 being observed at 5

minutes, 800 kg/m^3 observed at 10 minutes and an asymptotic limit of 1000 kg/m^3 reached at around 20 minutes of infiltration.[5] Because of the known geometry of the resonators and known mass, the device density can be directly calculated and compared to the previously reported curve. The porosity can be estimated from the device density.

For further dimensional and porosity analysis, cross-sections of the resonator devices should be imaged in a scanning electron microscope (SEM). Cross-sections of the circular resonators can be created using a focused ion beam to cut the device. The SEM images can show pores sizes created by the distinct carbon nanotube structures.[5]

4.3 Device Characterization

4.3.1 Mask and Resonator Device Design

Mask features include varying sizes of rings and disks anchored at four radially nodal points to square-shaped pads. (See Figure 4) It is anticipated that an insignificant displacement occurs at the nodal point when driven in the wine-glass mode of vibration. The anchors exhibit a tapering from the pad to the resonator disk or ring to decrease the cross-sectional area in hopes of decreasing clamping losses during operation. [2] Additionally, the pad may include a triangular cut-out pattern [3] at the point of connection to the anchor limb, to allow for the absorption of radially displacement as observed in the radial contour mode of vibration. During the manufacturing process, the mask features are left clear while chrome coats the rest of the square mask surface. This allows for a positive photoresist layer to be processed and set in the pattern of the devices, and leaving the rest of the photoresist layer to be sacrificed and removed in a subsequent processing step to be described herein. The pads will serve as contact points for the anchors as well as electrical contact points for actuation of the resonator.

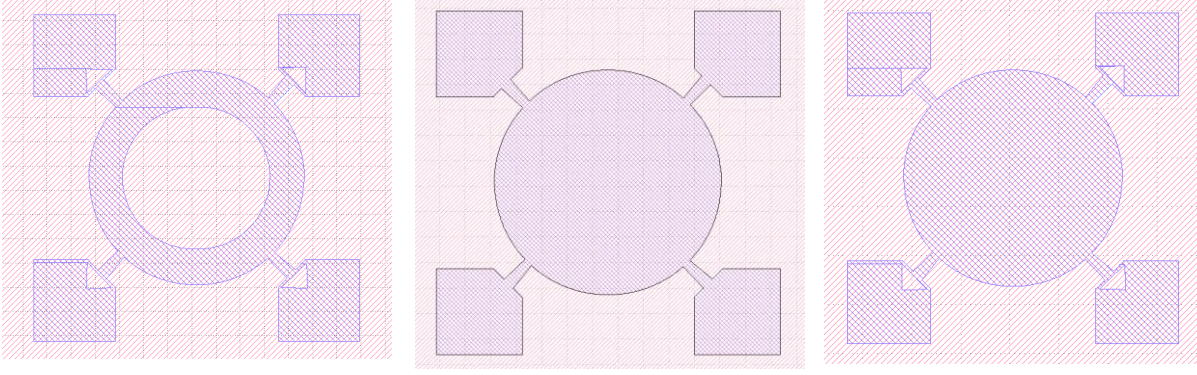


Figure 4: Snapshots of the resonator mask design file showing a variety of ring and disk structures.

4.3.2 Model for Circular Disks

The resonance frequency of a circular disk resonator can be derived from Bessel functions[21] of the following form:

$$\frac{J_0\left(\frac{\zeta}{\xi}\right)}{J_1\left(\frac{\zeta}{\xi}\right)} = (1 - \sigma) \quad (4.1)$$

$$\text{where, } \zeta = \omega_0 R \sqrt{\frac{\rho(2+2\sigma)}{E}}, \xi = \sqrt{\frac{2}{1-\sigma}} \quad (4.2)$$

Above, J_a are Bessel functions of the first kind of order a , $\omega_0 (= 2\pi f)$ is the angular resonance frequency, R is the radius of the disk, E is the Young's modulus, ρ is the mass density, and σ is the Poisson's ratio of the disk material. It has also been shown that the Bessel functions can be simplified to the following form for both radial contour[22] and wine-glass modes[23] of vibration:

$$f_0 = \frac{\omega_0}{2\pi} = \frac{\lambda_i}{2\pi R} \sqrt{\frac{E}{\rho(1 - \sigma^2)}} \quad (4.3)$$

where λ_i is the frequency parameter for the bulk mode, the values of which are provided in Table X for the first four modes.

4.3.3 Model for Annular Rings

The resonance frequency for an annular ring resonating in the bulk contour mode can be modeled by:

$$f_0 = \frac{n}{4L_s} \sqrt{\frac{E}{\rho}} \quad (4.4)$$

where L_s can be the length of radial center support beams or the inner radius of the ring. The outer radius can then be determined from Bessel functions of the first and second kinds.[4]

4.4 Resonance Predictions

Resonance frequencies were predicted for various configurations of the circular disks and rings resonators according to Equations (4.3) and (4.4), respectively. The Poisson ratio was assumed to be approximately 0.33.[15] A value for Young's Modulus has been reported for similar structures at 8.66 GPa.[15] This value was reported for structures grown on 4nm iron catalyst layer with infiltration times of 30 minutes corresponding to a material density of 1000 kg/m³. Lower density materials are much more flexible and may exhibit a lower Young's Modulus. The frequency parameter was assumed to be between 1.4-1.99 for the fundamental mode of vibration for the wine-glass mode and n was assumed to be 1 for the ring contour mode of vibration. Table 1 shows some predicted fundamental resonance frequencies for a sample set of circular disks that were infiltrated for 5 and 20 minutes corresponding to a material density of about 400 kg/m³ and 100 kg/m³, respectively.

Diameter of Circular Disk (um)	Predicted Fundamental Resonance Frequency (Mhz) 5 min infiltration	Predicted Fundamental Resonance Frequency (Mhz) 20 min infiltration
927	3.2	1.5
1187	1.8	1.2
1780	1.2	.78
2375	9.2	.59
2956	.74	.47
4550	.48	.31
8900	.25	.16

Table 1: Predicted resonance frequencies for various CNT-M disk resonant structures

4.5 Electro-Thermal Actuation

For higher pressure gaseous and liquid environments, a large force is needed to drive the resonator at the desired frequency. Because of its ability to deliver a large force, thermal actuation has proven to be a very effective method of transduction in non-vacuum environments[24] and was chosen to be the method of actuation for the CI-CNT disk and ring resonators. A proposed set up and process to drive the circular resonator via thermal actuation would be to bond very thin coil wires to at least two of the resonator pads via a conductive epoxy that would allow for electrical conductivity through the wire to the resonator structure. Each coil wire would be connected to a heat resistor, through which an alternating AC or DC current can be run to produce thermal waves throughout the circular resonator structure.

4.6 Resonance Testing

In most thermally-actuated devices, a preferred method of vibration measurement is through piezo-resistive elements because they can be simultaneously active in the existing

electrical circuit. However, an even more precise measurement of vibration and thus the resonant frequency can be achieved using a laser Doppler vibrometer (LDV). An LDV system usually comprises a two-beam laser interferometer that measures the frequency difference between an internal reference beam and a test beam. A beam from a laser is split into a reference beam and a test beam through a beamsplitter. The test beam undergoes a known frequency shift and is then directed to the resonator. The oscillating device produces a Doppler shift in the beam. Some of the light scattered by the resonator will be received by the LDV and directed to a photodetector via the beamsplitter. The photodetector provides a frequency modulated (FM) signal from which the velocity vs. time motion of the resonator can be determined, if desired. Advantages of the LDV system are the ability to make vibrations measurements without contact, without a physically attached transducer, and without mass-loading the target device.

Chapter 5

Results

5.1 Device Results

Circular resonators were fabricated with outer radii ranging from 900-8900 μm with anchor widths ranging from 40-430 μm and anchor lengths ranging from 115-1100 μm . The photolithography mask provided adequate resolution for the smallest feature sizes. The growth process was configured to be 15 minutes to achieve at least a 500 μm forest height, with a varying infiltration time between 5-20 minutes. Device density was predicted to be between 400-1000 kg/m^3 depending on infiltration time.[5] A sample was successfully released from the substrate using Method 1 and was re-mounted to the silicon wafer via carbon tape. The fabrication process is highly tunable and any of the aforementioned dimensions may be determined by manipulating various steps in the design and CNT-M fabrication process.

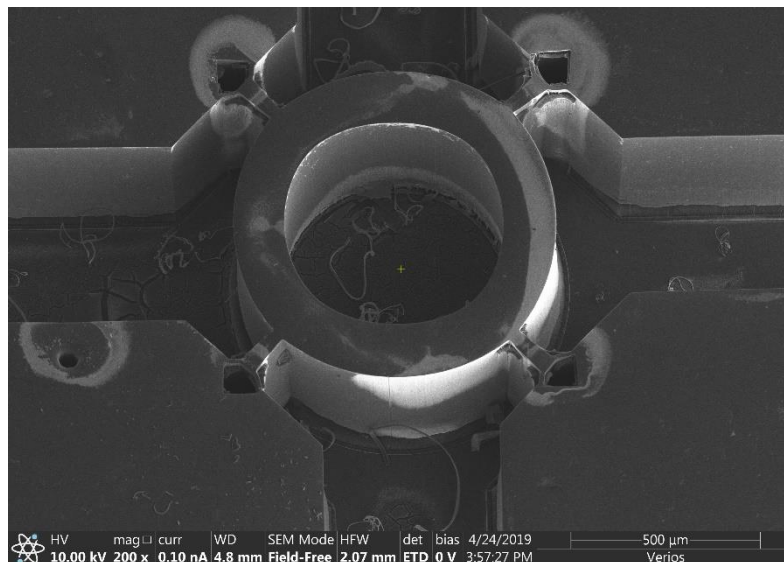


Figure 5: An image taken by a scanning electron microscope showing the detail of a ring resonator structure fabricated using the CNT-M process

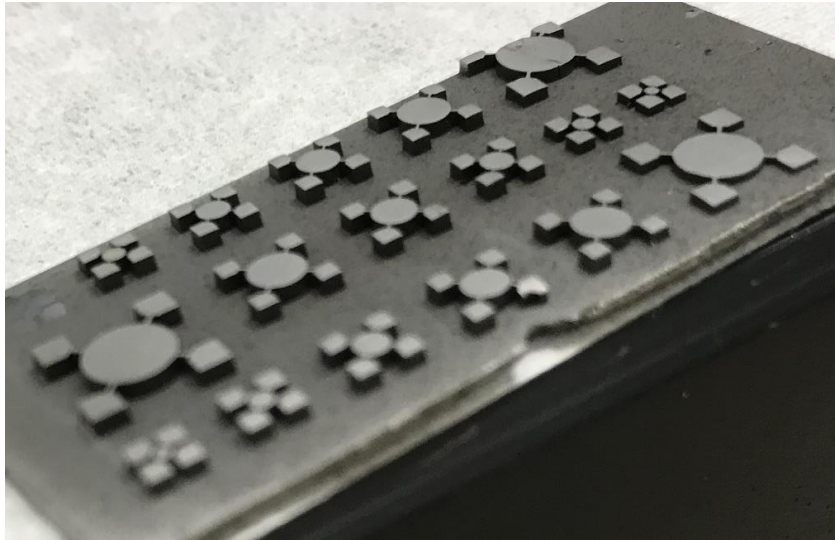


Figure 6: an array of CNT-M resonant structures grown for 15 minutes and infiltrated for 20 minutes.

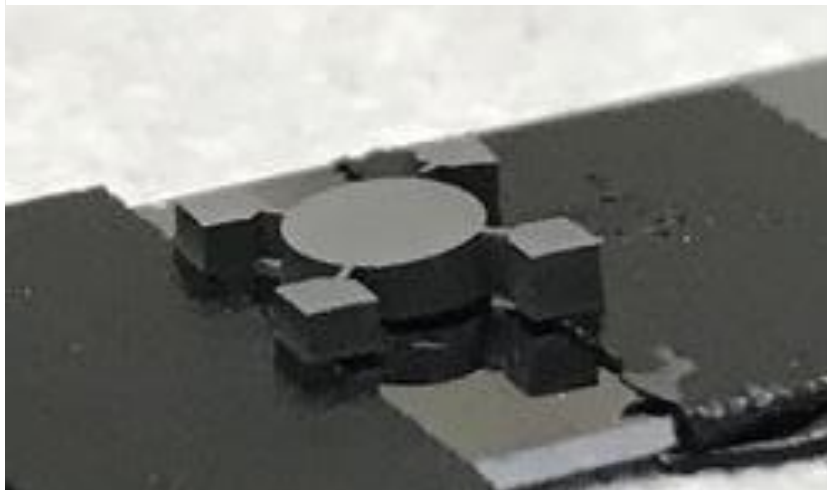


Figure 7: a photograph of a CNT-M disk resonator mounted to a silicon substrate via carbon tape to elevate the center portion of the structure so that it is free to oscillate.

5.2 Method of Release Results

Only a few of the methods were able to be tested for this study. Based on the etching rate and the time soaked in the KOH bath, Method 1 shows some promise in that the centers of the circular resonators have been released while maintaining contact under the pads. A sample (Sample 1) of the wafer housing several resonator rings was placed in a KOH bath for 33 minutes, rinsed for 30 seconds in a water bath, transferred to a second water bath, and then soaked in an acetone bath. (See Figures 8-10 for results on this release process). However, measurements have to be taken using the LDV to confirm successful release of a sample set of devices. A disadvantage of this method is that the titanium tip is too large to etch around the smaller disk and ring resonators. Several were broken during the process of manually etching. A single, larger ring was placed in the KOH bath for 55 minutes following Method 2. However, this length of time proved excessive and the entire ring was released from the silicon wafer substrate. On another disk resonator, some of the cyanoacrylate wicked onto the disk portion of the resonator device which will affect its ability to oscillate at its natural resonance frequency. A small copper wire was used to paint the pads, but a smaller diameter wire would prove to be more effective in preventing wicking into undesired locations of the device.

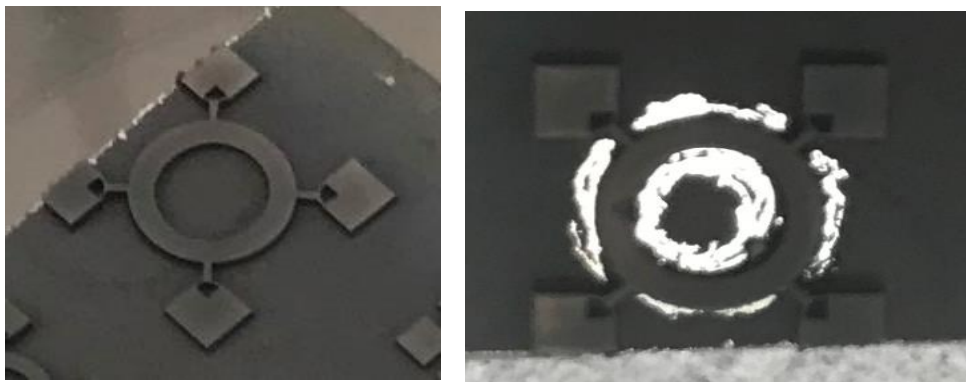


Figure 8: From left to right: a photograph of a CNT-M ring resonator after growth and infiltration having a carbon floor layer; a photograph of the same structure with some of the carbon floor layer scratched away to expose the silicon.

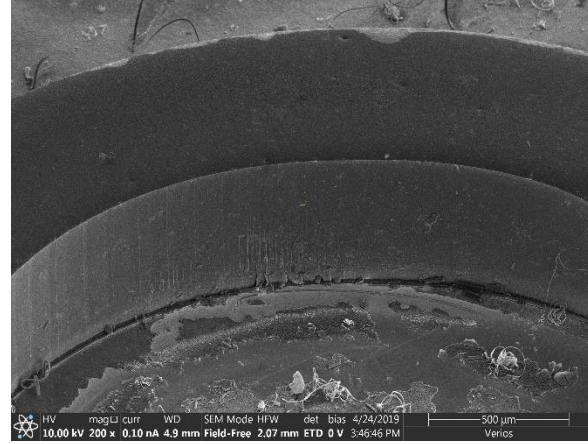
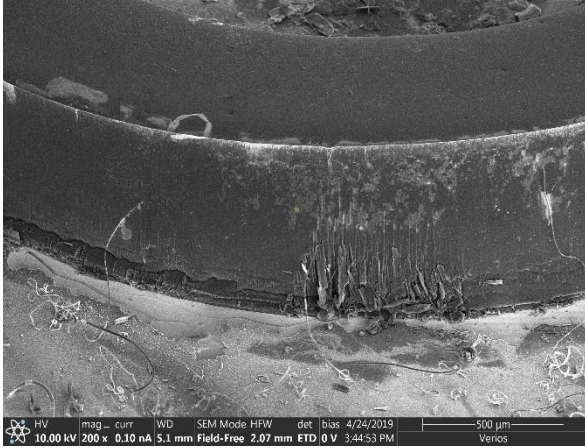


Figure 9: From left to right: an SEM image of the outside of a CNT-M ring resonator after Method 1 release process; the inside of a CNT-M ring resonator after Method 1 release process. From inspection, it appears at least a partial portion of the ring has been released successfully.

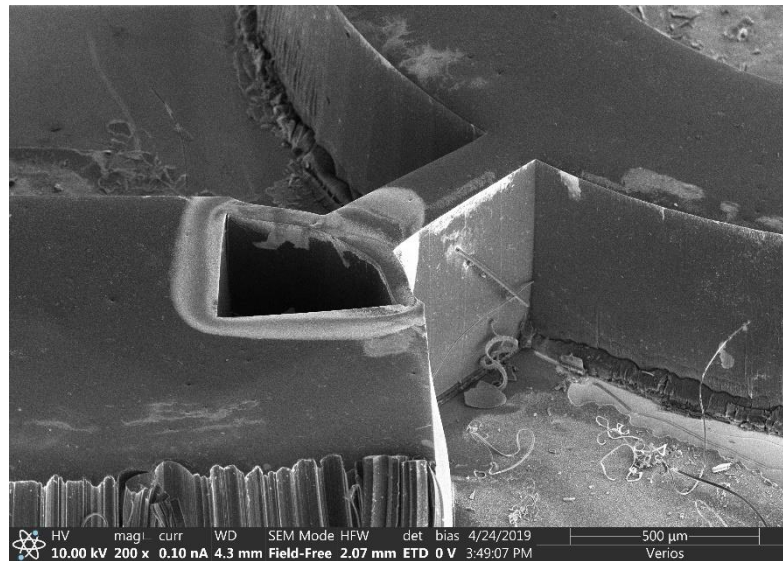


Figure 10: an SEM image of the anchor and pad features of a CNT-M ring resonator after the Method 1 release process.

5.4 Discussion

The porous circular resonators show theoretical promise as chemical sensors with high quality factors based on design parameters drawn from the background literature. Methods of releasing the device need to be further explored and experimented to determine the most effective way to release the desired portion of the resonator device. Measurements of the resonant frequency using the LDV were not able to be taken within the timeframe of this study. It is anticipated that the resonant frequencies and modes of vibration should be determined via the LDV internal shaker before thermal actuation is attempted as the driving force. The quality factor can then be determined by Equation (2.1). In the case of smaller diameter circular resonators, it may be possible to use Method 6 for release because it would be reasonable to have a high pad area to disk or ring area ratio.

6. Bibliography

- [1] J. Basu and T. K. Bhattacharyya, "Microelectromechanical resonators for radio frequency communication applications," *Microsyst. Technol.*, vol. 17, no. 10–11, pp. 1557–1580, Oct. 2011.
- [2] R. Abdolvand, B. Bahreyni, J. E.-Y. Lee, and F. Nabki, "Micromachined Resonators: A Review," *Micromachines*, vol. 7, no. 9, p. 160, Sep. 2016.
- [3] J. E.-Y. Lee and A. A. Seshia, "5.4-MHz single-crystal silicon wine glass mode disk resonator with quality factor of 2 million," *Sens. Actuators Phys.*, vol. 156, no. 1, pp. 28–35, Nov. 2009.
- [4] and, and, and C. T.- Nguyen, "Micromechanical 'hollow-disk' ring resonators," in *17th IEEE International Conference on Micro Electro Mechanical Systems. Maastricht MEMS 2004 Technical Digest*, 2004, pp. 821–824.
- [5] S. G. Noyce, R. R. Vanfleet, H. G. Craighead, and R. C. Davis, "High surface-area carbon microcantilevers," *Nanoscale Adv.*, vol. 1, no. 3, pp. 1148–1154, 2019.
- [6] J. Brotz, S. Reader, and D. T. Mukherjee, *at. .*
- [7] S. A. Chandorkar, M. Agarwal, R. Melamud, R. N. Candler, K. E. Goodson, and T. W. Kenny, "Limits of quality factor in bulk-mode micromechanical resonators," in *2008 IEEE 21st International Conference on Micro Electro Mechanical Systems*, 2008, pp. 74–77.
- [8] S. Trolier-McKinstry and P. Muralt, "Thin Film Piezoelectrics for MEMS," *J. Electroceramics*, vol. 12, no. 1, pp. 7–17, Jan. 2004.
- [9] "Resonant MEMS: Fundamentals, Implementation, and Application," *Wiley.com*. [Online]. Available: <https://www.wiley.com/en->

- us/Resonant+MEMS%3A+Fundamentals%2C+Implementation%2C+and+Application-p-9783527676354. [Accessed: 19-Apr-2019].
- [10] "Performance optimization of high order RF microresonators in the presence of squeezed film damping - ScienceDirect." [Online]. Available: <https://www.sciencedirect.com/science/article/pii/S092442471400257X?via%3Dihub>. [Accessed: 19-Apr-2019].
- [11] and, and, and and C. T.- Nguyen, "Series-resonant VHF micromechanical resonator reference oscillators," *IEEE J. Solid-State Circuits*, vol. 39, no. 12, pp. 2477–2491, Dec. 2004.
- [12] S. Pourkamali and and F. Ayazi, "VHF single crystal silicon capacitive elliptic bulk-mode disk resonators-part II: implementation and characterization," *J. Microelectromechanical Syst.*, vol. 13, no. 6, pp. 1054–1062, Dec. 2004.
- [13] A. Rahafrooz and S. Pourkamali, "Rotational mode disk resonators for high-Q operation in liquid," in *2010 IEEE SENSORS*, 2010, pp. 1071–1074.
- [14] Y. Hwang, F. Gao, A. J. Hong, and R. N. Candler, "Porous Silicon Resonators for Improved Vapor Detection," *J. Microelectromechanical Syst.*, vol. 21, no. 1, pp. 235–242, Feb. 2012.
- [15] W. C. Fazio, J. M. Lund, T. S. Wood, B. D. Jensen, R. C. Davis, and R. R. Vanfleet, "Material Properties of Carbon-Infiltrated Carbon Nanotube-Templated Structures for Microfabrication of Compliant Mechanisms," presented at the ASME 2011 International Mechanical Engineering Congress and Exposition, 2011, pp. 481–490.
- [16] Z. Hao, "Anchor Loss in MEMS/NEMS," in *Encyclopedia of Nanotechnology*, B. Bhushan, Ed. Dordrecht: Springer Netherlands, 2016, pp. 1–8.
- [17] G. Chen *et al.*, "Fabrication of High Aspect Ratio Millimeter-Tall Free-Standing Carbon Nanotube-Based Microelectrode Arrays," *ACS Biomater. Sci. Eng.*, Mar. 2018.

- [18] J. Yang *et al.*, “Effect of Oxygen Plasma Alumina Treatment on Growth of Carbon Nanotube Forests,” *J. Phys. Chem. C*, vol. 118, no. 32, pp. 18683–18692, Aug. 2014.
- [19] “Carbon-Nanotube-Templated Microfabrication of Porous Silicon-Carbon Materials with Application to Chemical Separations - Song - 2011 - Advanced Functional Materials - Wiley Online Library.” [Online]. Available: <https://onlinelibrary.wiley.com/doi/full/10.1002/adfm.201001851>. [Accessed: 19-Apr-2019].
- [20] “KOH Etching | BYU Cleanroom.” [Online]. Available: <https://cleanroom.byu.edu/KOH>. [Accessed: 19-Apr-2019].
- [21] J. R. Clark, W.-Hsu, M. A. Abdelmoneum, and C. T.-Nguyen, “High-Q UHF micromechanical radial-contour mode disk resonators,” *J. Microelectromechanical Syst.*, vol. 14, no. 6, pp. 1298–1310, Dec. 2005.
- [22] and S. Pourkamali and F. Ayazi, “VHF single-crystal silicon elliptic bulk-mode capacitive disk resonators-part I: design and modeling,” *J. Microelectromechanical Syst.*, vol. 13, no. 6, pp. 1043–1053, Dec. 2004.
- [23] S. Pourkamali, A. Hashimura, R. Abdolvand, G. K. Ho, A. Erbil, and F. Ayazi, “High-Q single crystal silicon HARPSS capacitive beam resonators with self-aligned sub-100-nm transduction gaps,” *J. Microelectromechanical Syst.*, vol. 12, no. 4, pp. 487–496, Aug. 2003.
- [24] J. H. Seo and O. Brand, “High Q -Factor In-Plane-Mode Resonant Microsensor Platform for Gaseous/Liquid Environment,” *J. Microelectromechanical Syst.*, vol. 17, no. 2, pp. 483–493, Apr. 2008.